NONLINEAR PRESTACK INVERSION USING THE REFLECTIVITY METHOD AND QUANTUM PARTICLE SWARM OPTIMIZATION

XINGYE LIU[1], XIAOHONG CHEN[2], LI CHEN[3] and JINGYE LI[2]

[1] *College of Geology and Environment, Xi'an University of Science and Technology, Shaanxi Provincial Key Laboratory of Geological Support for Coal Green Exploitation, Xi'an 710054, P.R. China. lwxwyh506673@126.com*
[2] *State Key Laboratory of Petroleum Resources and Prospecting, National Engineering Laboratory for Offshore Oil Exploration, China University of Petroleum-Beijing, Beijing 102249, P.R. China.*
[3] *BGP INC, China National Petroleum Corporation Southwest Geophysical Research Institute, Chengdu 610000, P.R. China.*

(Received May 21, 2019; revised version accepted March 9, 2020)

ABSTRACT

Liu, X.Y., Chen, X.H., Chen, L. and Li, J.Y., 2020. Nonlinear prestack inversion using the reflectivity method and quantum particle swarm optimization. *Journal of Seismic Exploration*, 29: 305-326.

The vectorized reflectivity method is an economical and reliable method for solving the elastic wave equation under a one-dimensional assumption. It can obtain the information of full wave field and accurately describe diverse propagation effects of the seismic wave. The inversion method based on the reflectivity method finds suitable inverted parameters by minimizing the error between the synthetic seismograms and observed seismic data. The non-linear inversion problem can be solved by a gradient-based method or a global optimization method. The former relies heavily on the staring model and is prone to fall into a local minima. The global optimization algorithms demand for an accurate and rapid calculation of the forward modeling. The vectorized reflectivity method satisfies these requirements. We introduce and improve the quantum particle swarm optimization algorithm (QPSO), which has significant advantages in global search, into seismic inversion based on the reflectivity method, developing a novel nonlinear prestack inversion method in angle gather domain. The vectorized reflectivity method is able to synthesize seismic records quickly and accurately. Using the QPSO relieves reliance on the initial model. The Cauchy distribution is introduced to combat the possible premature convergence. The benefits of the vectorized reflectivity method and QPSO are combined. We apply the technique to model data and field data, which demonstrates the feasibility and reliability of the new method.

KEY WORDS: prestack inversion, reflectivity method, wave propagation effects, quantum particle swarm optimization, elastic wave equation.

0963-0651/20/$5.00

IN UCTION

well known that pre
information. Elastic a
the observed and sy
ate forward modeling r
function. At preser
of prestack inversion
nate formulas (e.g., E
al., 2017). There are
nulate the primary ref
ns are often contamina
pensable to fully corre

reflectivity method and solved the objective function exploiting the Gauss-Newton method to improve the inversion accuracy. However, the method also relied heavily on the initial model. An inappropriate starting model often produces false appearance in the inverted results.

Most geophysical inversion problems are nonlinear. The above inversion methods solve the nonlinear problems by employing the gradient-based method. It is inevitable to compute Jacobian matrix or even Hessian matrix. Besides, it relies heavily on the initial model. If the initial model is inappropriate, often falls into local minima or even does not converge (Sen and Stoffa, 1991; Luo, 2007). The global optimization algorithm can overcome the above disadvantages. Sen and Stoffa (1991) efficiently combined simulated annealing and the Kennett recursive reflectivity method to invert the elastic attributes. Li and Mallick (2013, 2014), Padhi and Mallick (2013, 2014), Mallick and Adhikari. (2015) employed genetic algorithm to accelerate convergence based on the Kennett recursive algorithm and gained satisfied results on single trace. But as a completely nonlinear method, global optimization demands for a forward modeling that is accurate and can be quickly computed because the forward procedure will be executed a large number of times (Jia, 2005). The vectorized reflectivity method can meet the requirements. Therefore, it makes sense using the vectorized reflectivity method to synthesize prestack seismic records and using global optimization method to solve the inversion objective function. Liu et al. (2018) integrated the vectorized reflectivity method and genetic algorithm.

Among many global optimization methods (such as Yin and Hodges, 2007; Akça and Basokur, 2010; Liu, 2018; Garabito, 2018), particle swarm optimization (PSO) is widely used in seismic inversion because of simple operation and idea (Shaw, 2007; Huang, 2012; Cui, 2016; Barboza, 2018). The motion state of particles is described by speed and position together. The advantages of PSO is well known. It involves fewer control parameters and converges fast. However, it cannot cover the whole feasible search space thus is not able to assure global convergence because of limitation by the form of convergence and speed of particles, leading to an insufficient accuracy (Van den Bergh, 2002). To overcome this deficiency, Sun et al. (2004) proposed a quantum particle swarm optimization (QPSO) algorithm based on the wave function of quantum mechanics. In QPSO, particles can appear at any position in the search space with a certain probability rather than restricting by particle moving orbits and speed. It can prevent the situation that algorithm is terminated before the individual optimal solution has not been found due to the limited particle speed in few searches. In dealing with intractable problems, the behavior is greatly promoted (Sun et al., 2004, 2007).

Therefore, we introduce QPSO to solve the prestack inversion problem. QPSO has the advantages of fewer parameters, simple calculation, searching in full space and good convergence. Using QPSO to solve the objective function can overcome the shortcomings of gradient-based method. Benefiting from the advantages that it is computationally fast and accurate,

the vectorized reflectivity method in angle domain can meet the requirements of QPSO. To maintain the population diversity and prevent possible premature convergence (De Jong, 1975; Davis1991; Rudolph, 2001; Pandey et al., 2014), we also introduce Cauchy distribution that has a long tail and improve the QPSO. The proposed method fully integrates the advantages of the vectorized reflectivity method and QPSO. We briefly outline this method. Tests on model and field data demonstrate the robustness and reliability.

FORWARD MODELING BASED ON THE VECTORIZED REFLECTIVITY METHOD

Restricting to 1D, forward computation can be efficiently performed utilizing the reflectivity method that is an analytical method to solve the elastic wave equation. It can produce a synthetic seismic record that is close to the real situation because propagation effects of seismic wave are considered, including reflections, transmissions, multiples, etc. To use QPSO efficiently, a forward modeling method with fast and accurate calculation is needed. Attributing to the computational efficiency and complexity of the widely used reflectivity method based on Kennett recursive matrix algorithm (such as Fryer, 1980; Mallick and Frazer, 1987), a vectorized reflectivity method (Phinney, 1987; Liu, 2016; Chen, 2017) is employed. This algorithm simplifies the calculation and intensively reduces the computation time. The solution process is carried out in the frequency-slowness domain. Then, the reflection coefficients are transformed into the space-time domain or the intercept time-ray parameter domain by numerical integration method. Since the observed seismic data are in the angle gather domain. We execute the vectorized reflectivity method in angle-time domain according to the contributions of Liu et al. (2016).

Assuming a source point and multiple detectors are placed on the top of the first layer of a horizontal layered medium, the total reflection coefficient $R(\omega, p)$ in the frequency ω-slowness p-domain can be gained by a six-element vector $\mathbf{w}$ (Chen, 2017):

$$\begin{aligned} \mathbf{R}_{PP}(\omega, p) &= \frac{\mathbf{w}_0(4)}{\mathbf{w}_0(1)} \\ \mathbf{R}_{PS}(\omega, p) &= \frac{\mathbf{w}_0(5)}{\mathbf{w}_0(1)} \end{aligned}, \tag{1}$$

where $\mathbf{w}_0$ represents the total reflection response received on the ground, and $\mathbf{w}_n$ represents the total reflection response below the interface of the n-th layer:

$$\mathbf{w}_n = \begin{bmatrix} \Delta & -R_{SP}\Delta & -R_{SS}\Delta & R_{PP}\Delta & R_{PS}\Delta & |R|\Delta \end{bmatrix}^T . \tag{2}$$

R denotes the reflection coefficients, the two subscripts denote the type of incident wave and the type of reflected wave, respectively. P represents *P*-wave and *S* represents *S*-wave. Δ is a scaling factor. Assuming that the $(N+1)$-th medium is a half-space elastic medium under the *N*-th reflecting interface and there is no reflection wave, the response below the *N*-th medium is as follows:

$$\mathbf{w}_N = \begin{bmatrix} 1 & 0 & 0 & 0 & 0 & 0 \end{bmatrix}^T \quad . \tag{3}$$

A wave propagator matrix $\mathbf{Q}_n$ is employed to recursively compute the overall reflection response under the top interface starting from the bottom interface. Once $\mathbf{w}_0$ is obtained, the reflection coefficients in the frequency-slowness domain can be calculated according to eq. (1). The recursive process can be expressed as follows:

$$\begin{gathered} \mathbf{w}_0 = \mathbf{Q}_0\mathbf{w}_1,\ \mathbf{w}_1 = \mathbf{Q}_1\mathbf{w}_2,\ \mathrm{L}\ ,\ \mathbf{w}_n = \mathbf{Q}_n\mathbf{w}_{n+1},\ \mathrm{L}\ ,\ \mathbf{w}_{N-1} = \mathbf{Q}_{N-1}\mathbf{w}_N \\ \mathbf{Q}_n = \mathbf{T}_n^+\mathbf{E}_n\mathbf{T}_n^- \end{gathered} \tag{4}$$

where matrix $\mathbf{E}_n$ refers to a phase shift when seismic wave travels through layer *n*, and matrix $\mathbf{T}_n^+$ and $\mathbf{T}_n^-$ describe the influence of the medium above and below the n interface on the amplitude. They can be expressed as (Chen, 2017):

$$\mathbf{E}_n = diag\left[e^{-i\omega\Delta h\left(q_P+q_s\right)} \quad 1 \quad e^{-i\omega\Delta h\left(q_P-q_s\right)} \quad e^{i\omega\Delta h\left(q_P-q_s\right)} \quad 1 \quad e^{i\omega\Delta h\left(q_P+q_s\right)} \right] \tag{5}$$

$$\mathbf{T}_n^+ = \begin{bmatrix} t_{11} & t_{12} & t_{13} & -t_{13} & t_{15} & t_{11} \\ t_{21} & 0 & -t_{21} & -t_{21} & 0 & -t_{21} \\ t_{31} & t_{32} & t_{33} & -t_{33} & t_{35} & t_{31} \\ t_{31} & t_{42} & t_{33} & -t_{33} & t_{45} & t_{31} \\ t_{51} & 0 & t_{51} & t_{51} & 0 & -t_{51} \\ t_{61} & t_{62} & t_{63} & -t_{63} & t_{65} & t_{61} \end{bmatrix} \tag{6}$$

$$\mathbf{T}_n^- = \begin{bmatrix} t_{61} & t_{51} & t_{31} & t_{31} & t_{21} & t_{11} \\ -t_{65} & 0 & -t_{45} & -t_{35} & 0 & -t_{15} \\ -t_{63} & -t_{51} & -t_{33} & -t_{33} & t_{12} & -t_{13} \\ t_{63} & -t_{51} & t_{33} & t_{33} & t_{21} & t_{13} \\ -t_{62} & 0 & -t_{42} & -t_{32} & 0 & -t_{12} \\ t_{61} & -t_{51} & t_{31} & t_{31} & -t_{21} & t_{11} \end{bmatrix} , \tag{7}$$

where v_P and v_S denote P- and S-wave velocity respectively. Δh is the thickness of the n-th medium. $q_p = \sqrt{1/v_p^2 - p^2}$ and $q_s = \sqrt{1/v_s^2 - p^2}$ denote P- and S-wave slowness in vertical direction. Assuming $q = \sin\theta / v_p$ represents the horizontal slowness, $\Gamma = 2p^2 - 1/v_s^2$, $\mu = \rho v_s^2$, then we can get the sixteen independent components of $\mathbf{T}_n^+$ and $\mathbf{T}_n^-$:

$$
\begin{aligned}
&t_{11} = -\left(q^2 + q_p q_s\right)/\mu, t_{12} = -2qq_p/\mu, t_{13} = -\left(q^2 - q_p q_s\right)/\mu, t_{15} = -2qq_s/\mu,\\
&t_{21} = iq_s/\beta^2,\\
&t_{31} = -iq\left(\Gamma + 2q_p q_s\right), t_{32} = -4iq^2 q_p, t_{33} = -iq\left(\Gamma - 2q_p q_s\right), t_{35} = -2i\Gamma q_s,\\
&t_{42} = -2i\Gamma q_p, t_{45} = -4iq^2 q_s,\\
&t_{51} = -iq_p/\beta^2,\\
&t_{61} = -\mu\left(\Gamma^2 + 4q^2 q_p q_s\right), t_{62} = -4\mu\Gamma q q_p, t_{63} = -\mu\left(\Gamma^2 - 4q^2 q_p q_s\right), t_{65} = -4\mu\Gamma q q_s .
\end{aligned}
\tag{8}
$$

Subsequently, the reflection coefficient is integrated by frequency. The synthetic seismograms in $\tau - p$ domain can be output by convoluting the reflection coefficient in $\tau - p$ domain with seismic wavelet $\mathbf{S}(\omega)$:

$$
\mathbf{d}(\tau, p) = \frac{1}{2\pi}\int_{-\infty}^{\infty} \mathbf{S}(\omega)\mathbf{R}(\omega, p)e^{i\omega\tau}d\omega \quad . \tag{9}
$$

Since the obtained seismic records in prestack inversion are angle gathers, the reflection coefficient in frequency-slowness domain $\mathbf{R}(\omega, p)$ are resampled according to Snell's law to obtain the reflection coefficient in frequency-angle domain $\mathbf{R}(\theta, \omega)$ (Liu et al., 2016). The synthetic angle gathers are generated by fulfilling inverse Fourier transform after multiplying $\mathbf{R}(\theta, \omega)$ with seismic wavelet:

$$
\mathbf{d}(t, \theta) = \frac{1}{2\pi}\int_{-\infty}^{\infty} \mathbf{S}(\omega)\mathbf{R}(\theta, \omega)e^{i\omega t}d\omega \quad . \tag{10}
$$

In order to analyse the advantages of the reflectivity method, a test model that consists of five layers is constructed based on the Goodway model, as shown in Fig. 1 (mudstone appears in black and gas sandstone appears in grey). A Ricker wavelet with the main frequency of 30 Hz is employed to implement forward modeling. We briefly describe the differences of seismogram computed by the reflectivity method and the exact Zoeppritz equation. Fig. 2 displays the synthetic angle gathers and their difference. There are four main events corresponding to four interfaces of the model. At the same time, it can also be found that there are some events with weak energy in Fig. 2a because the reflectivity method can simulate multiple waves. However, there are no events of multiple waves in

Fig. 2b synthesized by exact Zoeppritz equation. For many actual data, the multiple reflection energy is often superimposed on primary reflection in thin interbedded reservoirs, which seriously decreases the resolution of seismic records. If this influence is neglected, deviation will be brought into inversion results. At different interfaces, amplitude of the events varies in Fig. 2a whose reflectivity method is used while that of the events in Fig. 3b that is outputted by the exact Zoeppritz equation keeps identical. The reason is that seismic wave will attenuate under the impact of various wave propagation effects. The reflectivity method takes this change into account whereas the Zoeppritz equation does not. Reflection amplitudes of these interfaces are extracted from the synthetic angle gathers for analysis. Amplitude of reflection events is exactly equal when the attributes of upper and lower layers are identical generated by using the Zoeppritz equation (Fig. 3b). In contrast, amplitude calculated by the reflectivity method is discrepant at different interfaces (Fig. 3a). Since the reflectivity method can simulate multiple waves and take into account various wave propagation effects, performance of the reflectivity method is preferable to the Zoeppritz equation.

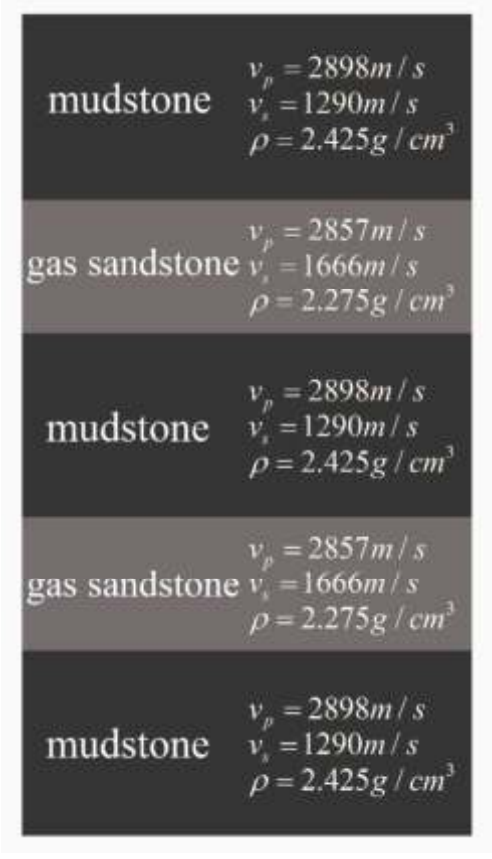

Fig. 1. The test model 1.

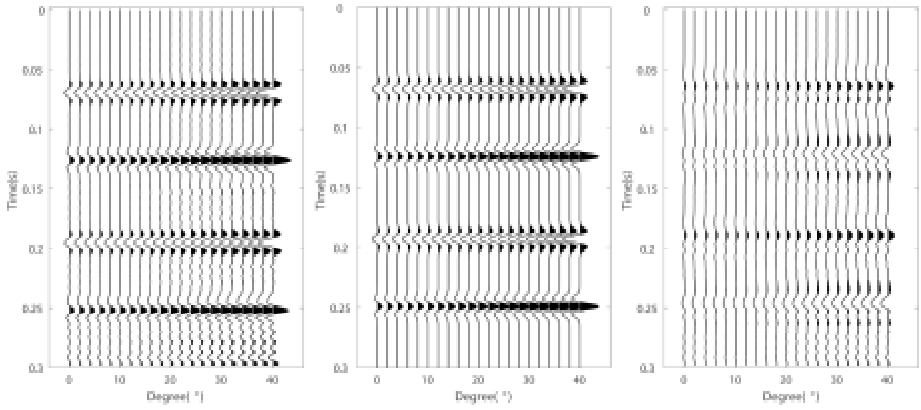

Fig. 2. Forward angle gathers synthesized by the reflectivity method (a) and Zoeppritz equation (b), respectively; (c) differences between the two forward angle gathers.

QUANTUM PARTICLE SWARM OPTIMIZATION ALGORITHM

The ultimate goal of this study is to invert P-wave velocity, S-wave velocity and density with a low dependency on initial model and a high accuracy. The inverse problem can be realized by minimizing the error between synthetic seismic records with actual data:

$$O = \left\| \mathbf{d}_{syn}(\theta, \mathbf{m}) - \mathbf{d}_{obs}(\theta) \right\|^2 \quad , \tag{11}$$

where $\mathbf{d}_{syn}(\theta, \mathbf{m})$ is the synthetic seismogram, $\mathbf{m}$ denotes the parameters to be inverted and $\mathbf{d}_{obs}(\theta)$ represents observed data.

As mentioned above, the gradient-based method to solving the objective function may converge to a local minimum rather than the global minimum if the starting model is inappropriate. In order to overcome the drawbacks of the gradient-based method, global optimization algorithm is employed. PSO algorithm is favored in a wide variety of scientific fields among various global optimization algorithms. PSO, theoretically, is relatively simple, involves few parameters and is easy to implement (Sun et al., 2007). But Van den Bergh (2002) has documented that PSO cannot guarantee global convergence. QPSO is a robust alternative, which attempts to endow quantum behavior to particles and remove the restriction of speed information on particles. The benefits of QPSO has been proved by Sun et al. (2004). QPSO is able to overcome the shortcomings of PSO. It also has few control parameters and is easy to operate. Moreover, the particle could appear in any position of the whole search space with a certain probability owing to introduce probability density function without the constraint of the fixed orbit. Only a brief summary of the QPSO is given here, more detailed can be found in Sun et al. (2004).

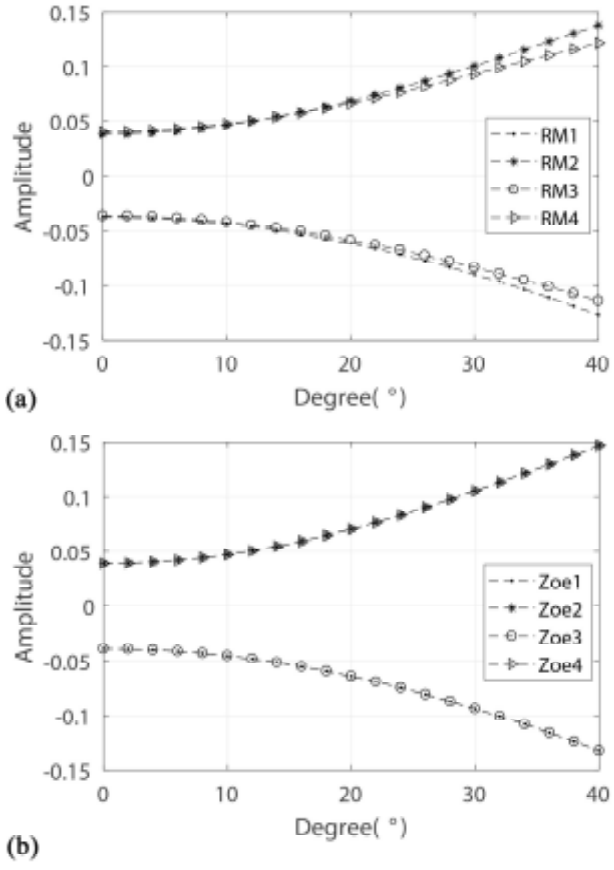

Fig. 3. Amplitude variation with angle of different reflective interfaces using different forward modeling method. (a) Reflectivity method; (b) Zoeppritz equation.

In QPSO, the state of particles is described by wave function. The probability density function of particles appearing at a certain point in the space is gained by solving Schrodinger equation. Then the position equation of particles is obtained by Monte Carlo stochastic simulation (Sun et al., 2004; Xu et al., 2005). For a *D*-dimensional space, the spatial position of the *i*-th particle among $\mathbf{X}=\{\mathbf{X}_1,\mathrm{L}\ \mathbf{X}_i,\mathrm{L}\ ,\mathbf{X}_M\}$ at the *t*-th iteration is $\mathbf{X}_i(t)=(X_{i1}(t),X_{i2}(t),\mathrm{L}\ ,X_{iD}(t))$, $i=1,2,\mathrm{L}\ ,M$, then the spatial position of this particle at the $t+1^{th}$ iteration is:

$$X_{ij}(t+1)=z_{ij}(t)\pm\lambda\left|C_j(t)-X_{ij}(t)\right|\ln\left(1/u_{ij}(t)\right) \quad , \tag{12}$$

where λ is a contraction factor that is the only parameter in QPSO, and

$u_{ij}(t)$ is a random number obeying uniform distribution. Assuming the individual optimal position is $\mathbf{Z}_i(t)=(Z_{i1}(t),Z_{i2}(t),\mathrm{L}\ ,Z_{iD}(t))$. The average optimal position of particle swarm $\mathbf{C}(t)=\sum_{i=1}^{M}\mathbf{Z}_i(t)\Big/M$ is introduced, which enables particles to wait for each other in the process of evolution and improves the ability of collaboration and global search. Suppose the global optimal position of the particle swarm is $\mathbf{G}(t)=\{G_1(t),G_2(t),\mathrm{L}\ ,G_D(t)\}$, $\varphi_j(t)$ is a random number obeying uniform distribution and $z_{ij}(t)$ denotes a local attractor that can be expressed as:

$$z_{ij}(t)=\varphi_j(t)Z_{i,j}(t)+[1-\varphi_j(t)]G_j(t) \quad . \tag{13}$$

Consequently, the formulas (12) and (13) together constitute the updating formulas of particle position. However, when disposing with complex high-dimensional optimization problems, the diversity of particles decreases gradually and premature convergence usually occurs with the increase of iterations. Cauchy distribution with a long tail in its probability densify function is introduced. In the original method, random numbers $u_{ij}(t)$ and $\varphi_j(t)$ obey uniform distribution, whereas we use the Cauchy distribution to generate random numbers, i.e., $u_{ij}(t)\sim C(1,0)$, $\varphi_j(t)\sim C(1,0)$. Because Cauchy distribution has the characteristic of "long tail" and has a wider distribution area, it helps to make the particle position appear far away from the local attractor, thus increasing the diversity of particles, reducing the occurrence of precocity phenomenon, and further improving the accuracy of global optimization.

To sum up, the flowchart of the new inversion method is inducted as Fig. 4.

INVERSION TEST ON MODEL DATA

Firstly, the prestack inversion method based on the reflectivity method integrating QPSO is carried out on a simple model. Information of the test model 1 is displayed in Fig. 1. The input seismic data (Fig. 5b) is computed using the vectorized reflectivity method (Fig. 2a), then random noise (Fig. 5a) with signal-to-noise ratio (SNR) of 1.5 is added. The inverted results exhibited in Fig. 6 – closely follow the parameters of the model, showing a good noise immunity. Fig. 7 shows the predicted seismic data and residual between it and the observed data (Fig. 5b). The residual is almost equal to the random noise, indicating its stability.

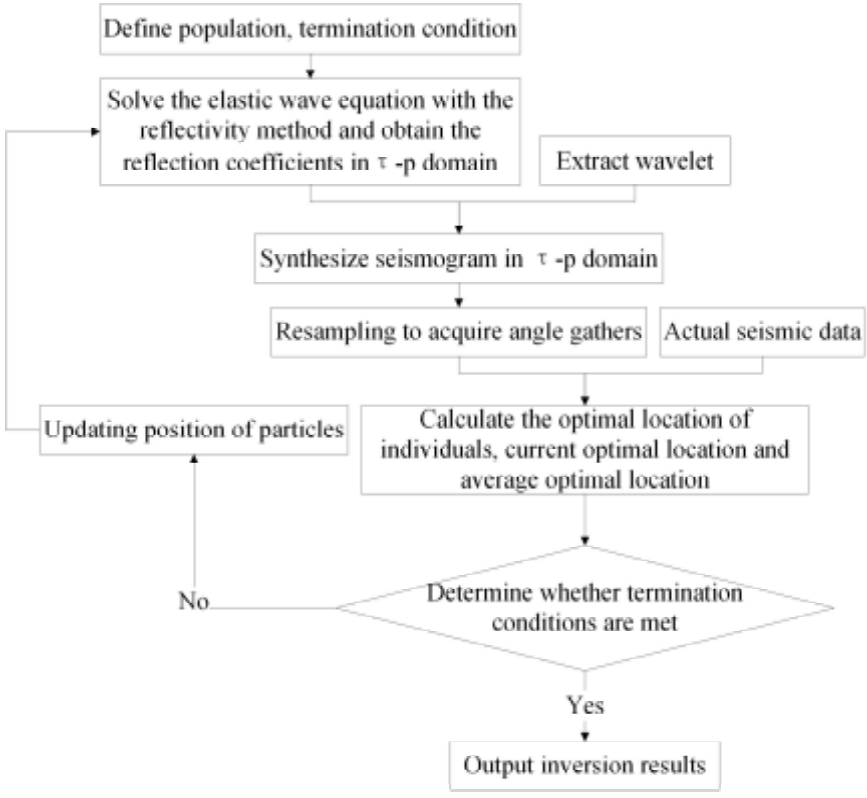

Fig. 4. Flowchart of the present method.

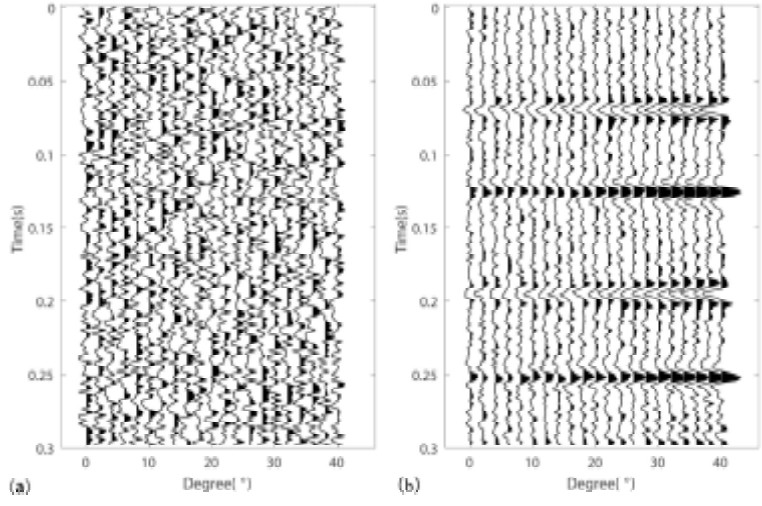

Fig. 5. Random noise (a) and the observed seismic data of test model 1 (b).

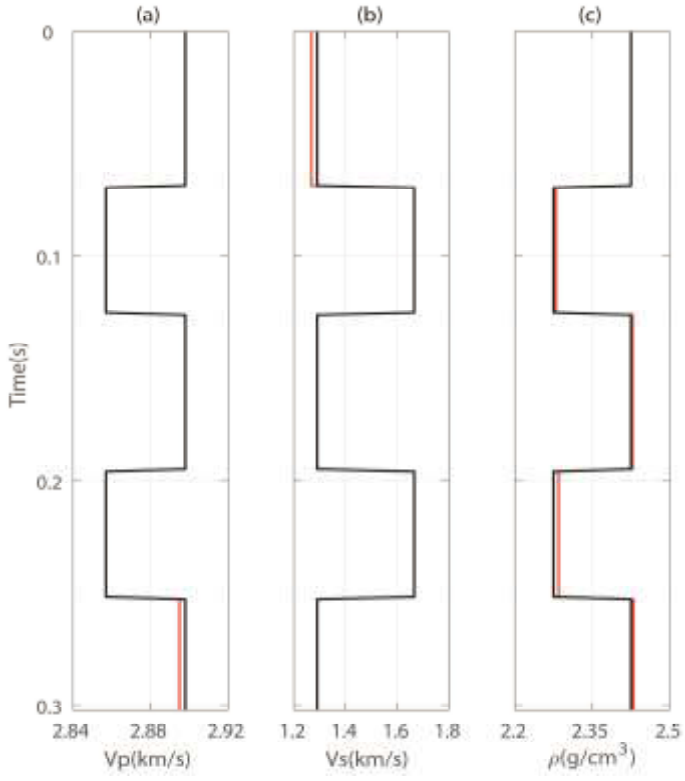

Fig. 6. The inversion results of test model 1, red curve represents the inversion results, and the black are the real model.

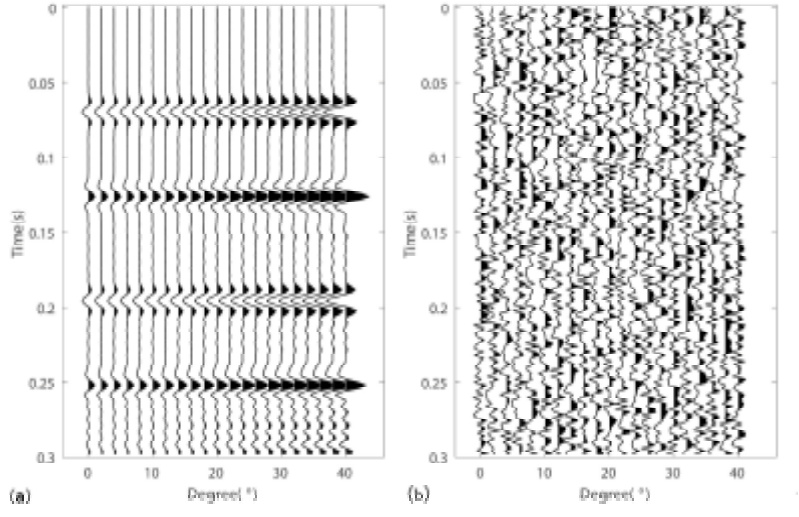

Fig. 7. The predicted seismogram (a) and residual (b) between it and input seismic data (Fig. 5b).

Next, the section of gas reservoir and oil reservoir in Marmousi2 model is extracted for further illustrating the validity of the present method. The real elastic attributes of the test model are shown in Fig. 8. The arrows indicate the location of oil and gas reservoirs respectively. The elastic parameters of oil and gas reservoirs are different from those of surrounding rocks, especially the distinction of P-wave velocity and density is dramatic. The "observed" seismic data is generated by convolving of the reflection coefficient calculated by the vectorized reflectivity method with a 30 Hz Ricker wavelet and adding random noise with SNR of 2.

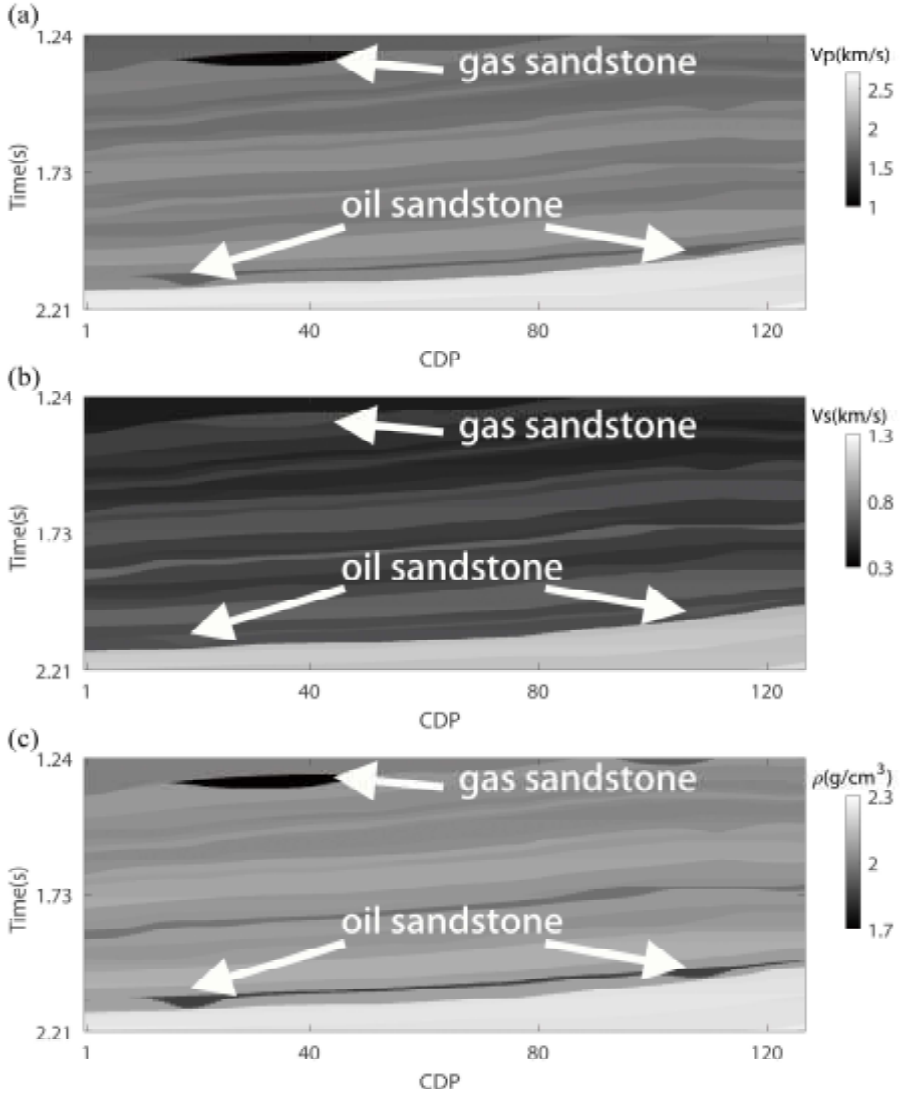

Fig. 8. Test Model 2 (from Marmousi2 model).

From the stack seismogram displayed in Fig. 9, apparently, the gas-bearing sandstone at the top of the model has significant seismic response characteristics. However, the seismic response characteristics of oil-bearing sandstone in the deep layer are weak, which make its identification problematic. Although QPSO is independent of the starting model and the initial population can be randomly produced, we borrow the prior information, such as log and geological data etc., for generating the initial population (Dariu et al., 2003; Liu et al., 2018). The purpose is to accelerate convergence, prevent precocity and restrict the search space with a low-frequency tend. The inverted results by using the proposed method are shown in Fig. 10. Fig. 10a is the inverted profile of P-wave velocity, in which morphology of the target oil and gas reservoir are similar with the original model. The oil and gas reservoirs are weakly reflected in the inverted S-wave velocity profile (Fig. 10b), while the main stratigraphic and lithologic interfaces can be well distinguished, which is consistent with the knowledge that S-wave velocity can indicate lithology. The oil and gas reservoirs are distinctly indicted in density inversion results (Fig. 10c) because density is directly related to fluid information.

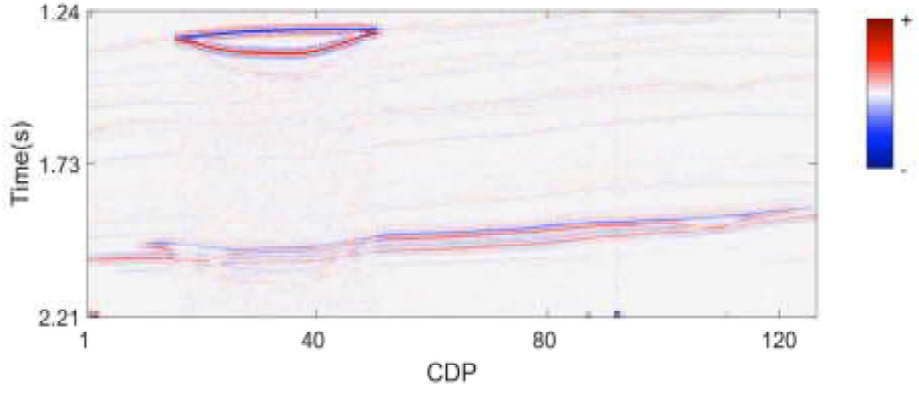

Fig. 9. The stack profile of the test model 2.

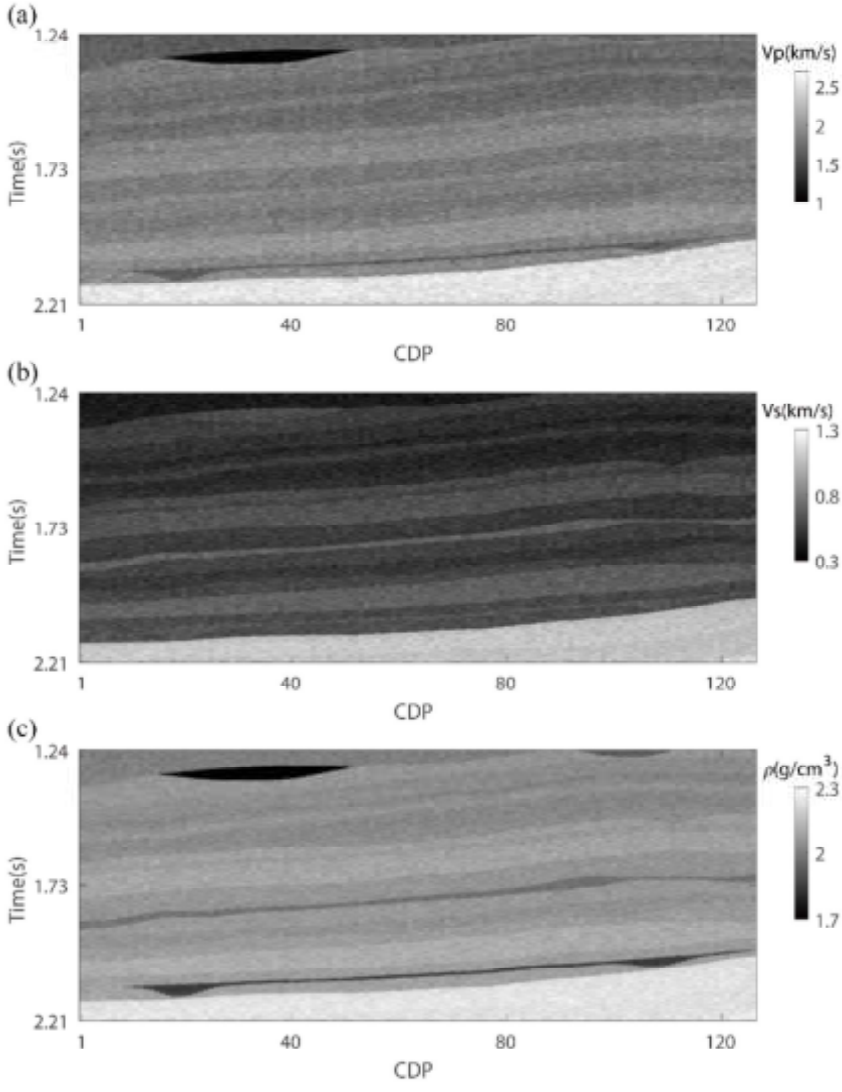

Fig. 10. The inversion result of the test model 2 using the present method.

FIELD DATA APPLICATION

The method is applied to a single well at first. Real logging curves of the well are exhibited in Figs. 11a-c with black lines. Angle gathers including 21 traces with angles ranging from 0 to 40 are shown in Fig. 12. A Ricker wavelet of 30 Hz is used to calculate it. A random noise with SNR of 2 is added. Then, the synthetic seismogram computed by present method is employed to match the angle gathers. With the help of the advantages of QPSO, the inversion results (shown with the red lines in Figs. 11a-c are in good agreement with the true values of logging curves. Another reason

[redacted]

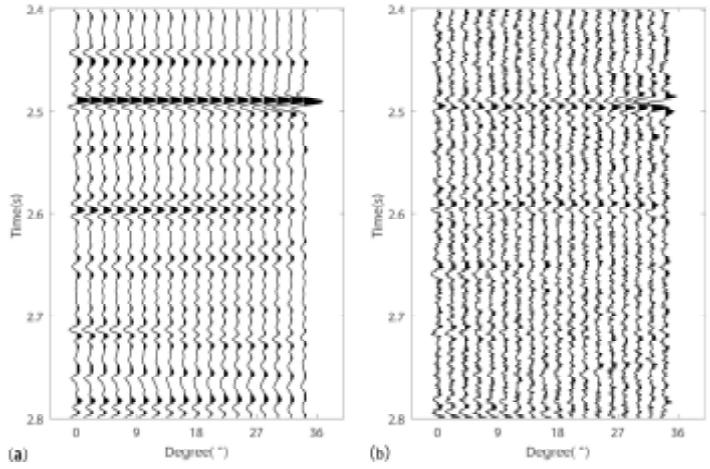

Fig. 13. The predicted angle gathers (a) and residual (b) between it and input gathers (Fig.12c).

Ultimately, we apply the method to a seismic section from a Chinese onshore exploration area. The target reservoir is structural-lithologic composite reservoirs formed in the lacustrine environment during the Late Cretaceous-Early Tertiary period. The sand-shale interbedded is developed at the top of the target reservoir. As a result, the seismic wave is severely affected by multiple waves and transmission loss, which seriously influence the accuracy of reservoir prediction and pose challenges for the exploration and development of the target reservoirs. In this study, 60 prestack CDPs between 2100 and 2300 milliseconds are used. For each CDP, angle gathers ranging from 3 to 34 degrees are available. The seismic data have been processed according to a routine workflow without suppressing multiples and compensating transmission loss. Fig. 14 displays the poststack seismogram of the study area. The layered structural characteristics are noticeable. In actual exploration, there is an economical oil and gas well at the 13th CDP location.

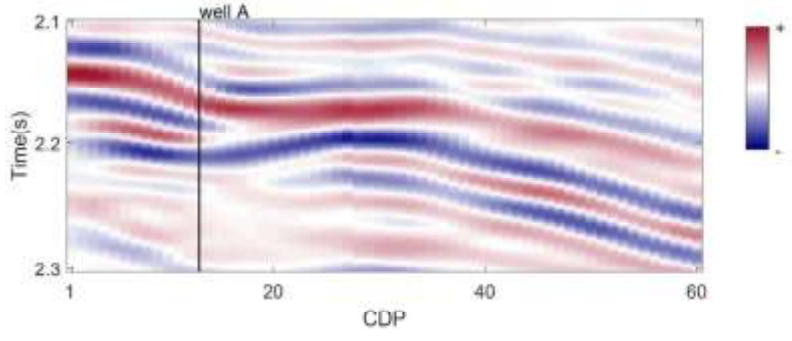

Fig. 14. The seismogram of the filed data.

Seismic wavelets for different angles are extracted from the angle traces of actual seismic data (shown in Fig. 15). They are employed for inversion with the angle gathers of 3 to 8, 9 to 18, 19 to 28 and 29 to 34 degrees, respectively. The final inverted P-wave velocity, S-wave velocity and density are output and shown in Fig. 16. From the inversion results, it is worth mentioning that the inversion results effectively identify different formations, which are consistent with the shape reflected in stack gather. The inversion results are consistent with the trend revealed in well logging curves (black lines in the Fig. 16), which demonstrates the method can keep a good performance in practice and effectively proves the practicability of the method.

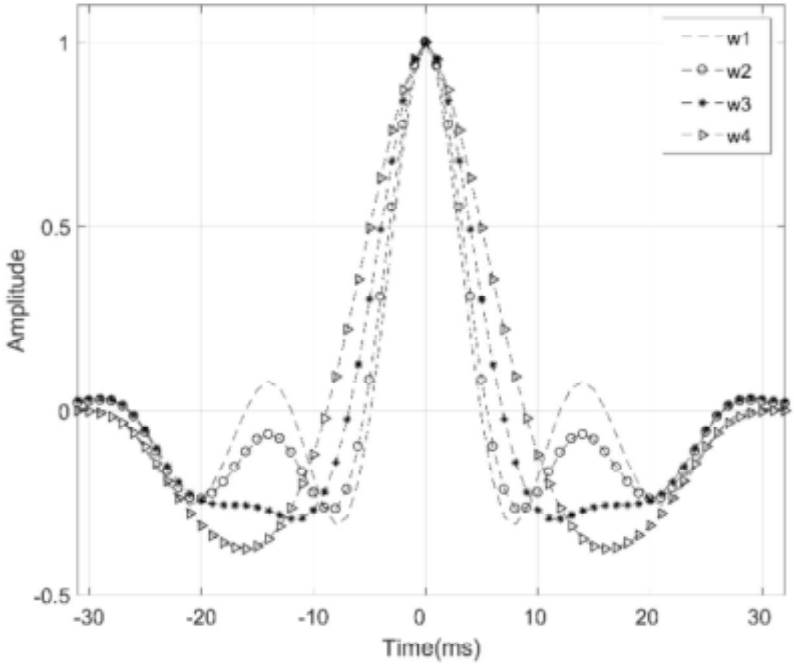

Fig. 15. Seismic wavelet extract from angle gathers.

CONCLUSION

We describe a new nonlinear prestack inversion method based on the vectorized reflectivity method. Under one-dimensional assumption, the reflectivity method can simulate the wave propagation effects, consider the influence of transmission loss and multiple wave on seismic response, and weaken the processing requirement of amplitude. The main advantage of the vectorized reflectivity method is the fast and accurate calculation, which satisfies the demand of global optimization. The objective function is solved nonlinearly by using the improved QPSO. Introducing the Cauchy distribution with a long tail helps to enhance the diversity of solutions and

prevent precocity occurrence in the process of solving. Both the application examples on model data and field data produce promising results, which offer proof for the stability and practicability of the proposed approach. The method can be easily generalized to multicomponent joint prestack inversion if the corresponding seismic data can be acquired and processed appropriately.

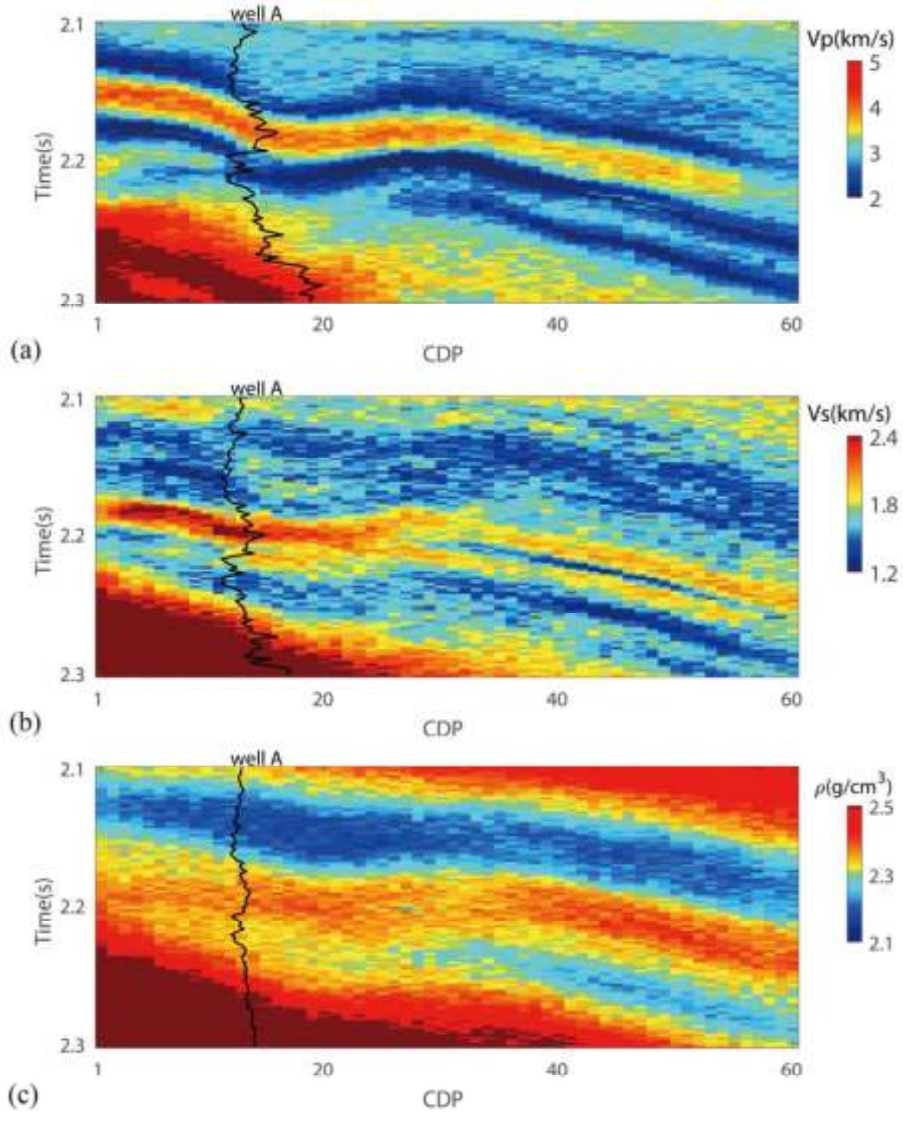

Fig. 16. Inversion results of the filed data by the present method: (a) P-wave velocity; (b) S-wave velocity; (c) density.

However, the vectorized reflectivity method we achieved is a single-channel inversion method without considering lateral correlation in the isotropic media. Relevant methods considering lateral correlation and methods for anisotropic media will be studied in the next work. With the addition of anisotropic parameters, the dimension of inversion problem is further increased. How to improve the computational efficiency at no cost of inversion accuracy will become a major problem. Besides, various advanced techniques that can avoid the precocity need to be further systematically studied.

ACKNOWLEDGMENT

This work is financially supported by the National Natural Science Foundation of China (41774129, 41774131, 41904116), the Foundation Research Project of Shaanxi Provincial Key Laboratory of Geological Support for Coal Green Exploitation (MTy2019-20). Finally, we would like to thank the reviewers and the journal's editors for their excellent suggestions and insightful comments.

REFERENCES

Akça, I. and Basokur, A.T., 2010. Extraction of structure-based geoelectric models by hybrid genetic algorithms. Geophysics, 75(1): F15-F22.

Barboza, F.M., Medeiros, W.E. and Santana, J.M.. 2019. A user-driven feedback approach for 2D direct current resistivity inversion based on particle swarm optimization. Geophysics, 84(2): E105-E124.

Buland, A., and Omre, H., 2003. Bayesian linearized AVO inversion. Geophysics, 68(1): 185-198.

Chen, L., 2017. Prestack AVO Inversion Based on the Reflectivity method using Bayesian theory. China University of Petroleum-Beijing.

Ciucivara, A. and Sen, M.K., 2009. A reflectivity method for laterally varying media. Expanded Abstr., 79th Ann. Internat. SEG Mtg., Houston: 2707-2711.

Cui, X., Gao, J., Zhang, B. and Wang, Z., 2016. Poststack impedance inversion using improved particle swarm optimization. Expanded Abstr., 86th Ann. Internat. SEG Mtg., Dallas: 3809-3813.

Dariu, H., Garotta, R. and Granger, P.Y., 2003. Simultaneous inversion of PP and PS wave AVO/AVA data using simulated annealing. Expanded Abstr., 73rd Ann. Internat. SEG Mtg, Dallas: 120-123.

Davis, L., 1991. Handbook of Genetic Algorithms. Van Nostrand Reinhold, New York.

De Jong, K., 1975. An analysis of the behavior of a class of genetic adaptive systems. Ph. D. Thesis, University of Michigan.

Fryer, G.J., 1980. A slowness approach to the reflectivity method of seismogram synthesis. Geophys. J. Internat., 63: 747-758.

Fuchs, K. and Müller, G., 1971. Computation of synthetic seismograms with the reflectivity method and comparison with observations. Geophys. J. Internat., 23: 417-433.

Garabito, G., 2018. Global optimization strategies for implementing 3D common-reflection-surface stack using the very fast simulated annealing algorithm: Application to real land data. Geophysics, 83(4): V253-V261.

Gouveia, W.P. and Scales, J.A., 1998. Bayesian seismic waveform inversion: Parameter estimation and uncertainty analysis. J. Geophys. Res., Solid Earth, 103(B2): 2759-2779.

Huang, K.Y., Shen, L.C., Chen, K.J. and Huang, M.C., 2012. Particle swarm optimization in multilayer perceptron learning for well log data inversion. Expanded Abstr., 82nd Ann. Internat. SEG Mtg., Las Vegas: 1-5.

Jia, Y.G., Li, X.F., Zhang, M.G., Li, X.F. and Wang, T.K., 2005. Summarization of research on seismic wave nonlinear inversion method. J. Disast. Prev. Mitigat. Engineer., 25: 345-351.

Kennett, B.L.N., 1979. Theoretical reflection seismograms for elastic media. Geophys. Prosp., 27: 301-321.

Kennett B.L.N., 1983. Seismic Wave Propagation in Stratified Media. Cambridge University Press, Cambridge.

Li, T. and Mallick, S., 2013. Prestack waveform inversion of four-component, two-azimuth surface seismic data for orthorhombic elastic media parameters using a nondominated sorting genetic algorithm. Expanded Abstr., 83rd Ann. Internat. SEG Mtg., Houston: 3283-3287.

Li, T. and Mallick, S., 2014. Prestack waveform inversion of three-component, two-azimuth surface seismic data for azimuthally dependent anisotropic parameters using a parallelized nondominated sorting genetic algorithm. Expanded Abstr., 84th Ann. Internat. SEG Mtg., Denver: 3205-3210.

Liu, H., Li, J., Chen, X., Hou, B. and Chen, L., 2016. Amplitude variation with offset inversion using the reflectivity method. Geophysics, 81(4): R185-R195.

Liu, W., 2017. The research of pseudo-wells' construction method using a fast non-dominated sorting genetic algorithm. China University of Petroleum-Beijing.

Liu, X., Li, J., Chen, X., Guo, K., Li, C., Zhou, L., and Cheng, J., 2018. Stochastic inversion of facies and reservoir properties based on multi-point geostatistics. J. Geophys. Engineer., 15: 2455-2468.

Liu, W., Wang, Y.C., Li, J.Y., Liu, X.O. and Xie, W., 2018. Prestack AVA joint inversion of PP and PS waves using the vectorized reflectivity method. Appl. Geophys., 15: 448-465.

Luo, H.M., 2007. Quantum genetic algorithm and its application to inversion of geophysics. China University of Geosciences.

Ma, Y., Loures, L. and Margrave, G.F., 2004. Seismic modeling with the reflectivity method. CREWES Research Report, 16-1.

Mallick, S. and Frazer, L.N., 1987. Practical aspects of reflectivity modeling. Geophysics, 52: 1355-1364.

Mallick, S. and Frazer, L.N., 1990. Computation of synthetic seismograms for stratified azimuthally anisotropic media. J. Geophys. Res. - Solid Earth, 95(B6): 8513-8526.

Mallick, S. and Adhikari, S., 2015. Amplitude-variation-with-offset and prestack-waveform inversion: A direct comparison using a real data example from the Rock Springs Uplift, Wyoming, USA. Geophysics, 80(2): B45-B59.

Müller, G., 1985. The reflectivity method - a tutorial. J. Geophys., 58: 153-174.

Padhi, A. and Mallick, S., 2013. Accurate estim[redacted]

Sen, M.K. and Roy, I.G., 2003. Computation of differential seismograms and iteration adaptive regularization in prestack waveform inversion. Geophysics, 68: 2026-2039.

Shaw, R. and Srivastava, S., 2007. Particle swarm optimization: A new tool to invert geophysical data. Geophysics, 72(2): F75-F83.

Sun, J., Feng, B. and Xu, W., 2004. Particle swarm optimization with particles having quantum behavior. Proc. 2004 Congr. Evolution. Computat., Portland, OR: 325-331.

Sun, J., Liu, J. and Xu, W., 2007. Using quantum-behaved particle swarm optimization algorithm to solve non-linear programming problems. Internat. J. Comput. Mathemat., 84: 261-272.

Van den Bergh, F. and Engelbrecht, A.P., 2002. A new locally convergent particle swarm optimiser. IEEE Internat. Conf. Systems, Man Cybernet., Tunis: 3-6.

Xu, W. and Sun, J., 2005. Adaptive parameter selection of quantum-behaved particle swarm optimization on global level. Internat. Conf. Intellig. Comput., Hefei, China: 420-428.

Yin, C. and Hodges, G., 2007. Simulated annealing for airborne EM inversion. Geophysics, 72(4): F189-F195.

Zhao, H., Ursin, B. and Amundsen, L., 1994. Frequency-wavenumber elastic inversion of marine seismic data. Geophysics, 59: 1868-1881.

Zhou, L., Li, J., Chen, X., Liu, X. and Chen, L., 2017. Prestack AVA inversion of exact Zoeppritz equations based on modified Trivariate Cauchy distribution. J. Appl. Geophys., 138: 80-90.